Electronic Supplementary Material (ESI) for ChemComm.

Electronic Supporting Information

Restricted-magnesium-vapor-reduction of amorphous SiO/C precursors to polycrystalline Si/SiO_x/C hybrid anodes

Jun Zhang, [b †] Fan Zhang, [a †] Wenqiang Zhu, [a] Xiaoming Xi, [b, *] Lezhi Yang, [b] Feiyue Tu, [b] Qingge Feng, [b] Tingting Li, [a] Yahui Yang, [a] and Lishan Yang [a, *]

[a] Key Laboratory of Chemical Biology & Traditional Chinese Medicine Research (Ministry of Education of China), National and Local Joint Engineering Laboratory for New Petrochemical Materials and Fine Utilization of Resources, Key Laboratory of the Assembly and Application of Organic Functional Molecules of Hunan Province, Hunan Normal University, Changsha, Hunan 410081, P. R. China.

[b] Changsha Research Institute of Mining and Metallurgy Co Ltd., Changsha 410012, P.R. China.

† These authors contributed equally to this work.

Corresponding authors:
Tel./Fax.: +86 731 88872531
E-mail addresses:
lsyang.chemistry@gmail.com; lsyang@hunnu.edu.cn (Lishan Yang),
xixiaoming@vip.163.com (Xiaoming Xi).

Author Contributions:

Jun Zhang: Data curation, Writing – original draft. **Fan Zhang**: Data curation, Writing – original draft, Formal analysis, Funding acquisition. **Weiqiang Zhu**: Data curation. **Xiaoming Xi**: Conceptualization, Project administration, Funding acquisition, Supervision. **Lezhi Yang**: Resources, Supervision. **Feiyue Tu**: Resources, Funding acquisition. **Qingge Feng**: Resources. **Tingting Li**: Formal analysis. **Yahui Yang**: Resources, Funding acquisition. **Lishan Yang:** Project administration, Writing – review & editing, Data curation, Supervision, Funding acquisition.

Materials and methods

In a typical process, 3.5 g SiO@C (SC, purchased from Btr New Material Group Co., D50 is 5.6 μm) and 1.2 g metal Mg powder (D50 is 61 μm) were separated and layered, placed in a designed graphite crucible, and the graphite crucible (20 mL) was placed in a tubular furnace, heated at 850 °C under argon atmosphere (flow rate controlled at 100 mL min^{-1}) with a heating rate of 5 °C min^{-1}, then held for 6 h. After cooling to room temperature, the mixture was washed with 2 M HCl solution for 6 h to remove redundant by-products. Finally, the samples were washed with distilled water several times, then vacuumized and dried at 60 °C for 12 hours to obtain SC-MG.

3.5 g SiO@C and 1.2 g metal Mg powder (D50 is 61 μm) were placed in an agate mortar and manually stirred for 0.5 h, placed in a designed graphite crucible, then through the same steps above to obtain SC-MP as a comparison sample.

Material Characterizations

The phase and crystallinity of the obtained samples were analyzed by powder X-Ray Diffraction (XRD Bruker D8 X-ray diffractometer, Cu Kα radiation, λ= 1.5406 Å, operated from 20° to 80° (2θ)) and Raman spectroscopy with 532 nm excitation laser (Raman, Thermo-Nicolet ALMECA, Holland). The hydrophilicity and contact angle of samples were analyzed by spinningdrop interface tensiometer (TX500 TM). The morphologies and element composition of the obtained samples were characterized by scanning electron microscope (SEM) (JSM-6490LV, Japan) and transmission

electron microscope (TEM, FEI Tecnai G2 F20). The sample with the section diagram was prepared by a Leica 3-x ion beam cutting system with copper foil on the substrate to protect the samples from helium beam damage. X-ray photoelectron spectroscopy (XPS, Thermo Scientific K-Alpha) was used to analyze the elements and components on the surface of the prepared samples. The specific surface area (BET, Quantachrome Autosorb-I) was used to analyze the change of the porosity of composites.

Electrochemical Measurements

To measure the electrochemical performance of SC-MG and SC-MP samples, type 2032 coin-type half cells were assembled. The active materials, super-P and sodium alginate (SA) were mixed at the weight ratio of 6:2:2 in deionized water to form homogenous slurry. Then the slurry was painted onto a copper foil, followed by drying at 100 °C for 12 h. The mass loading of active material for each electrode was about 1 mg cm^{-2}. The half cell was assembled by using metal lithium as the reference electrode and counter electrode in an Ar-filled glove box (O_2, H_2O<0.1 ppm). The electrolyte is made up of 1 M $LiPF_6$ dissolved in EC:DEC=1:1 (volume ratio) with 5% FEC. The galvanostatic discharge-charge measurements of the coin cells were tested on a LAND instrument (CT2001A, China) with a voltage range of 0.005-1.5 V at room temperature. The cyclic voltammetry (CV) and electrochemical impedance spectroscopy (EIS) were performed on an electrochemical workstation (CHI760E, China). EIS was measured over the frequency range of 100000 Hz to 0.01 Hz. CV characterizations with different scanning rate were conducted in the potential range of 0.01-2.0 V at a scan rate of 0.1 mV s^{-1} to 0.6 mV s^{-1}.

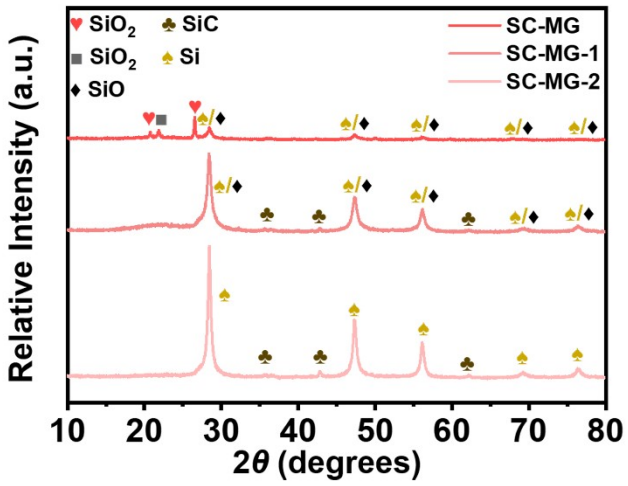

Fig. S1 XRD patterns of SC-MG samples with different proportions of SC and Mg.

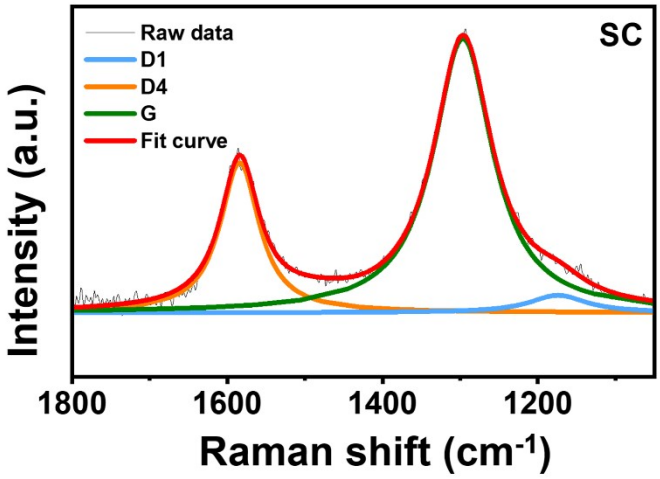

Fig. S2 Raman spectrum of SC.

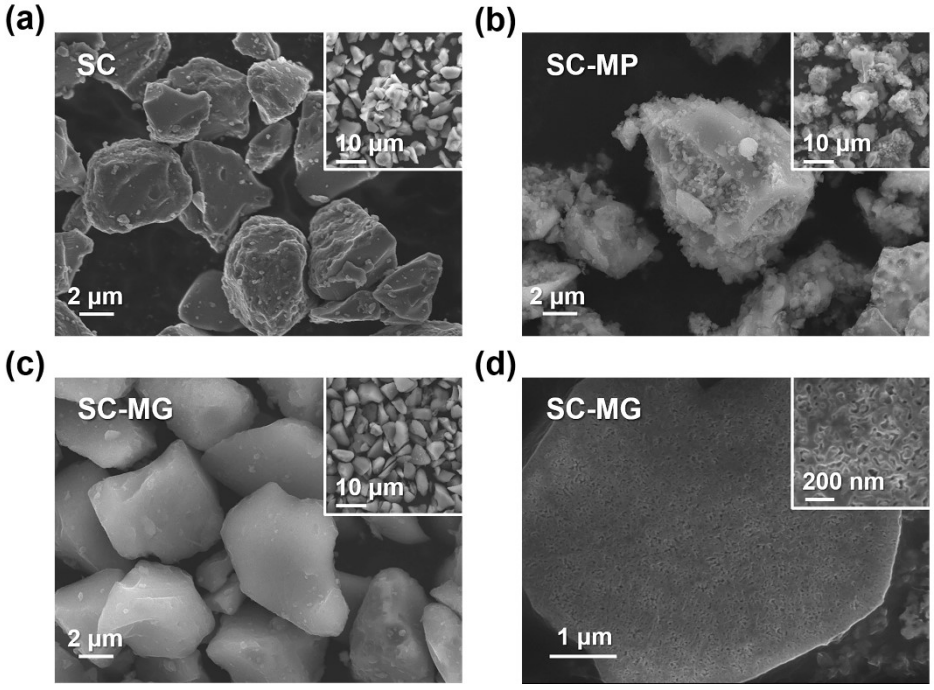

Fig. S3 SEM images of (a) SC, (b) SC-MP, and (c, d) SC-MG.

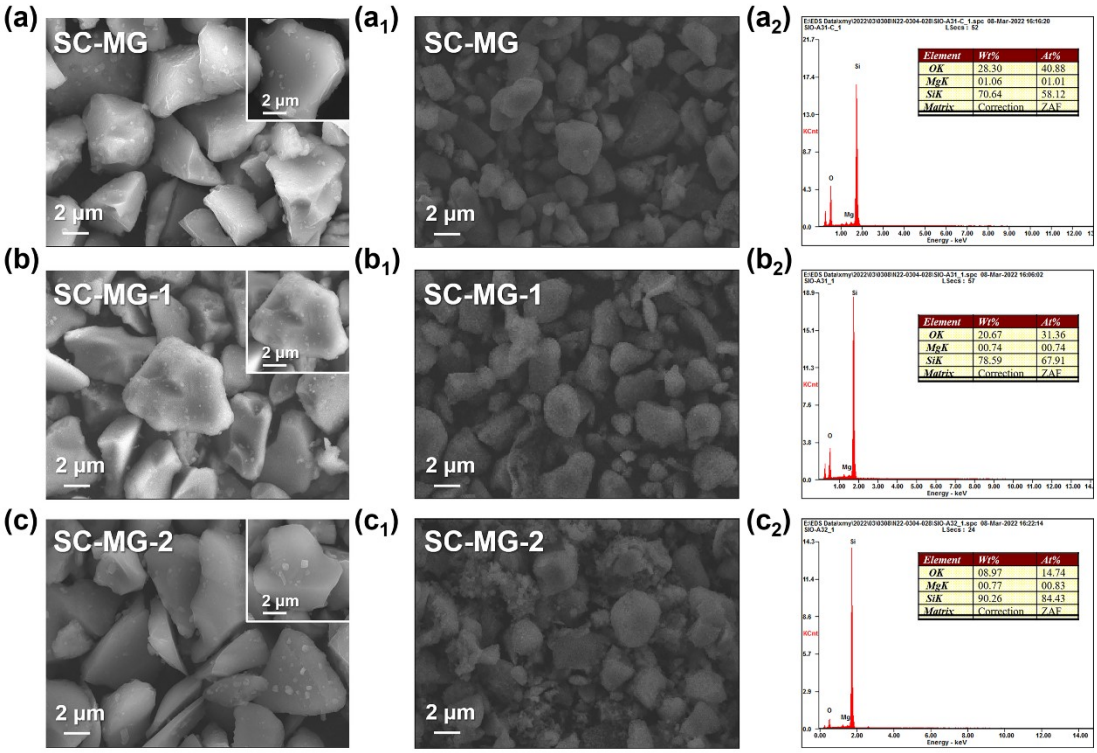

Fig. S4 SEM images of (a) SC-MG, (b) SC-MG-1, and (c) SC-MG-2.

With the increase of the ratio of Si-Mg, the magnesiothermic reduction carried out more thoroughly. It can be clearly observed that the particles surface gradually becomes rough, and the particles are obviously destroyed with the further increase of the ratio of Si-Mg. As shown in EDS mapping, the oxygen content in the products increased gradually.

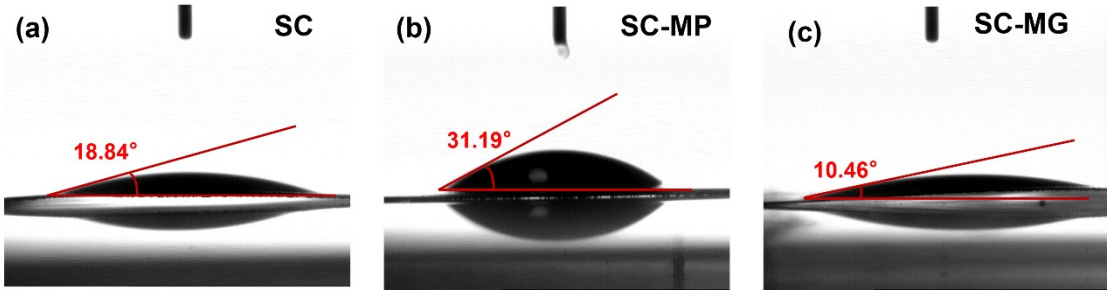

Fig. S5 The contact angle of electrodes with SC, SC-MP and SC-MG.

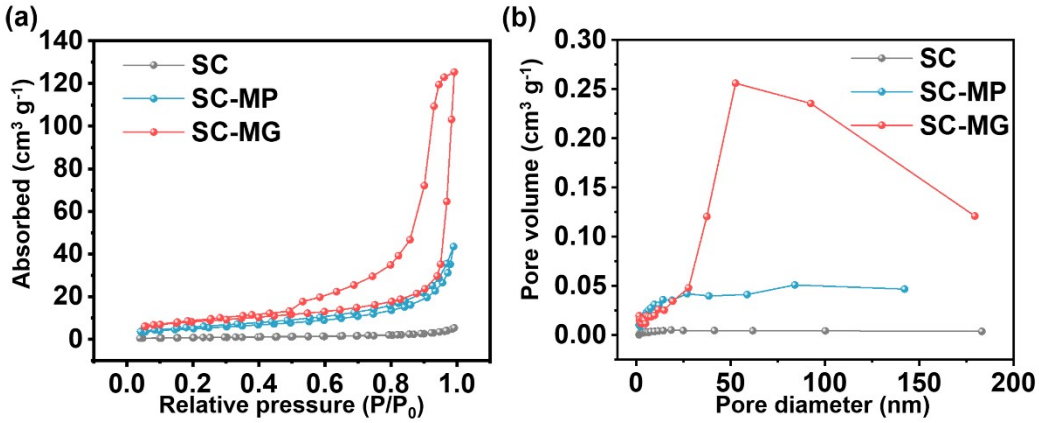

Fig. S6 (a) Nitrogen adsorption and desorption isotherms of SC, SC-MP, and SC-MG. (b) The corresponding pore size distribution of SC, SC-MP, and SC-MG.

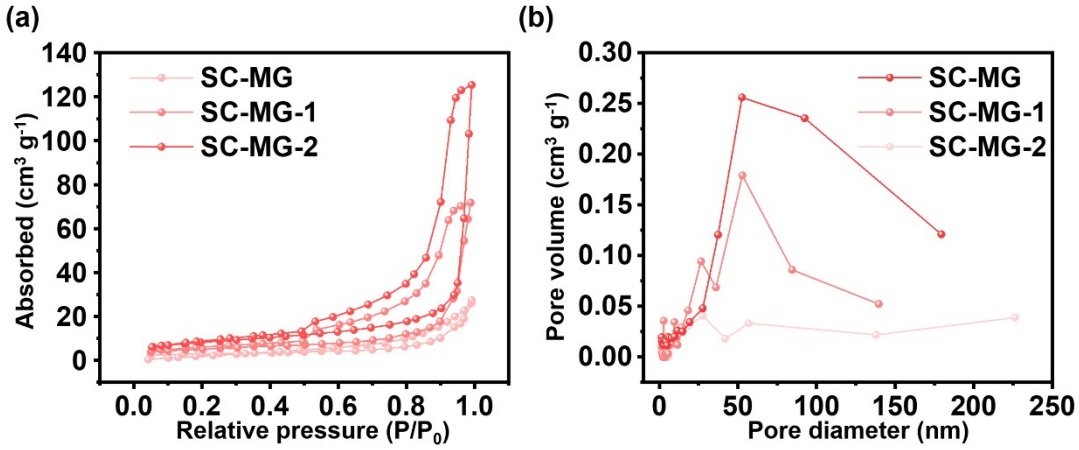

Fig. S7 (a) Nitrogen adsorption and desorption isotherms of SC-MG with different proportions of SC and Mg. (b) The corresponding pore size distribution of SC-MG with different proportions of SC and Mg.

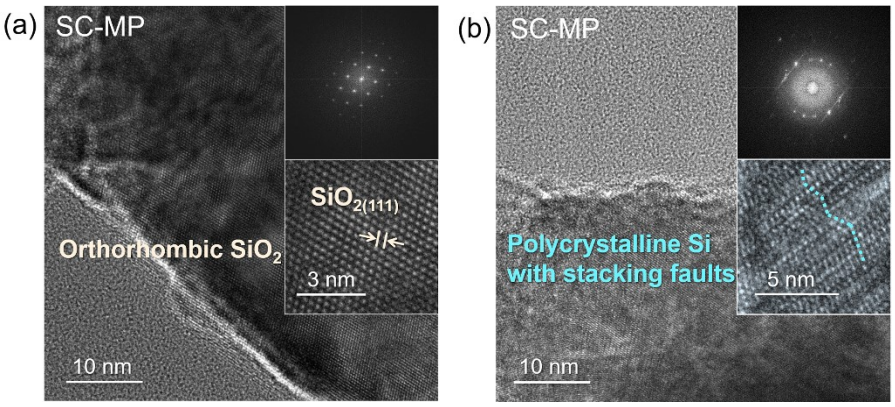

Fig. S8 HRTEM images of SC-MP and the corresponding SAED.

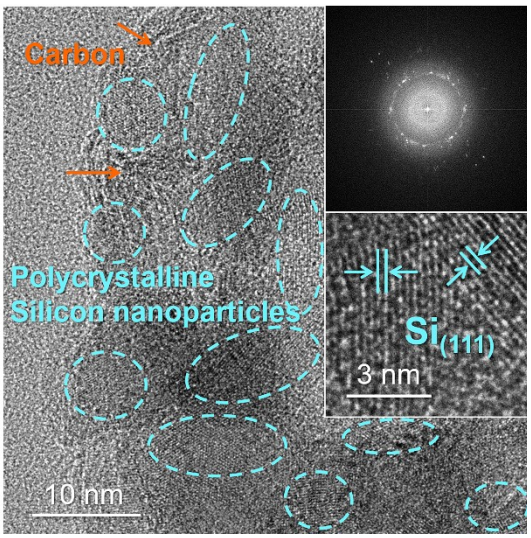

Fig. S9 HRTEM images of SC-MG and the corresponding SAED.

The presence of polycrystalline silicon nanoparticles and amorphous carbon layer observed in Fig. S9 further demonstrates that the successful synthesis of polycrystalline Si/SiO_x/C hybrid composites.

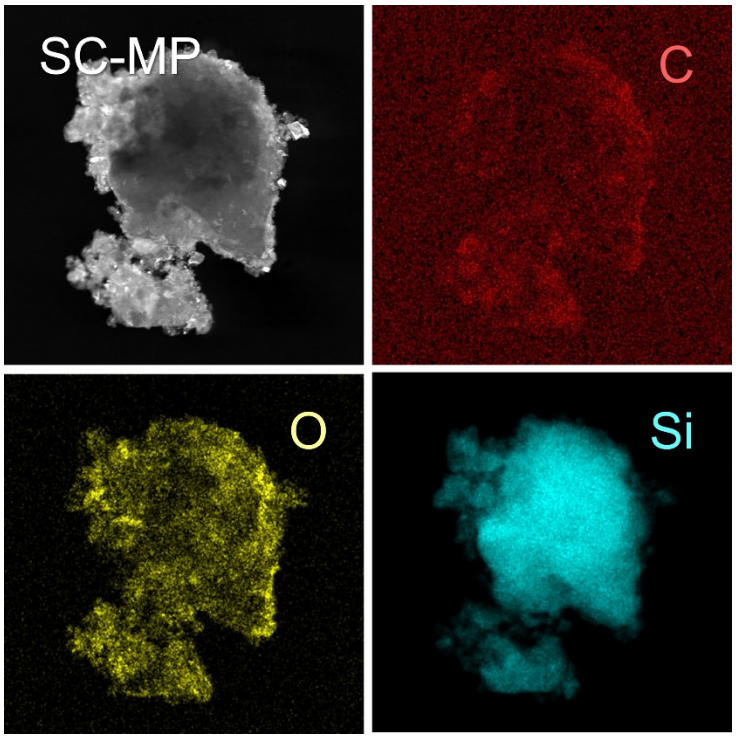

Fig. S10 EDS elemental mappings of SC-MG of Si, O and C.

The element distribution of SC-MP is shown in Fig. S10. The signal of Si significantly stronger than that of SC-MG, which indicates that the violence of Mg-powder-reduction.

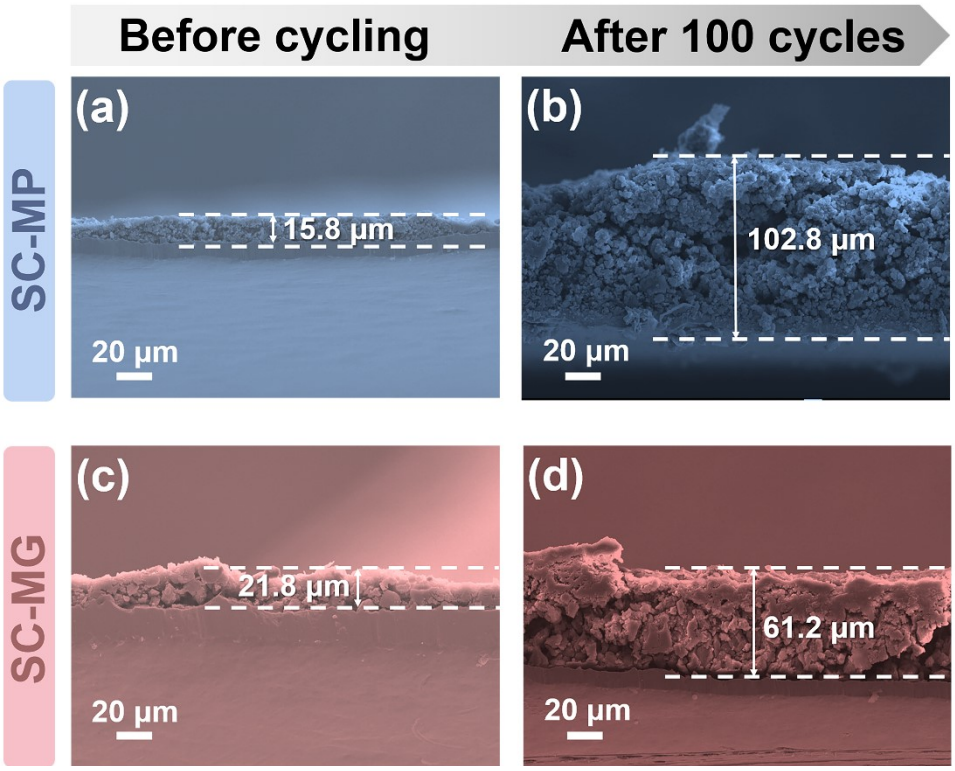

Fig. S11 Cross-sectional SEM images of the SC-MP and SC-MG electrodes at different cycles: (a) before cycling of SC-MP electrode, (b) after 100 cycles of SC-MP electrode, (c) before cycling of SC-MG electrode, and (d) after 100 cycles of SC-MG electrode.

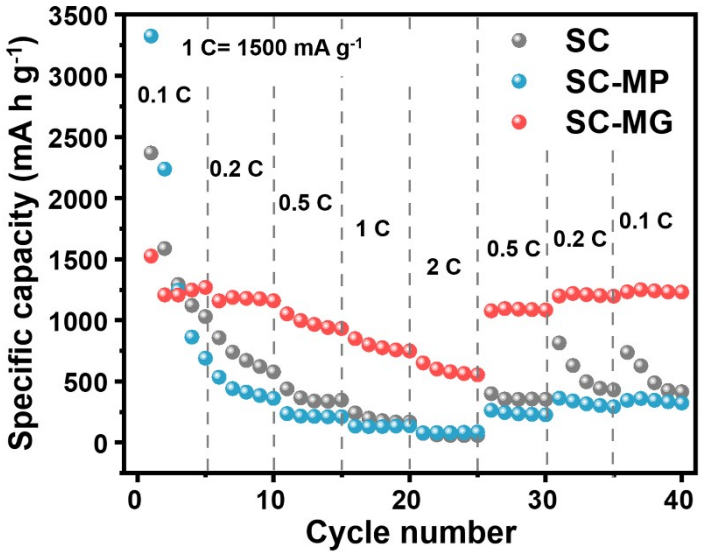

Fig. S12 Rate performance of SC, SC-MP and SC-MG anodes.

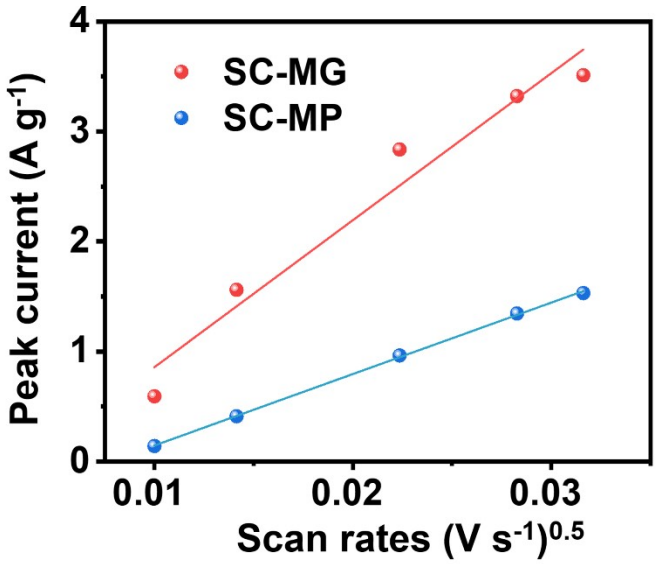

Fig. S13 Linear fits for the anodic peak current versus square root of scan rate of electrodes with SC-MP and SC-MG anodes.

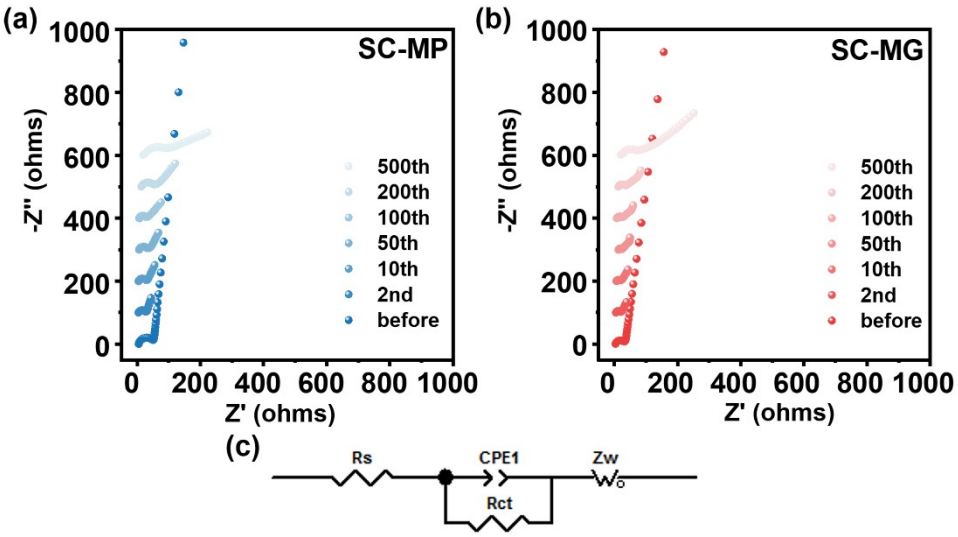

Fig. S14 EIS test with different cycles: (a) SC-MP anode, (b) SC-MG anode. (c) Analog circuit diagram corresponding to EIS results.

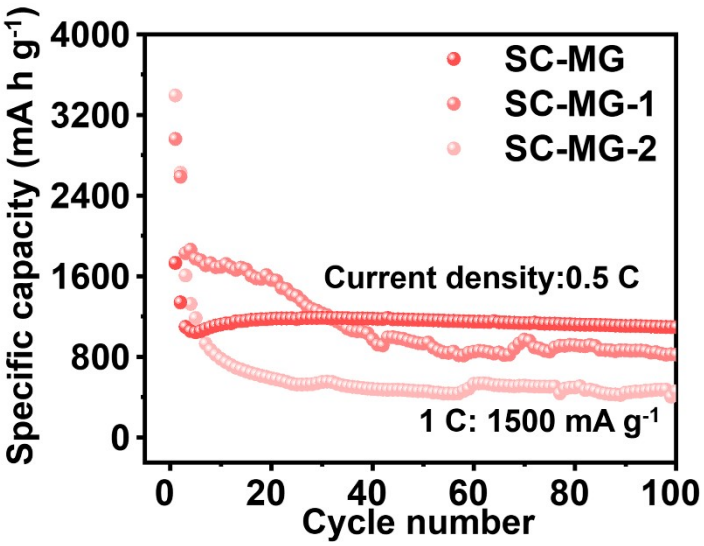

Fig. S15 Cycling performance of SC-MG anodes with different proportions of SC and Mg.

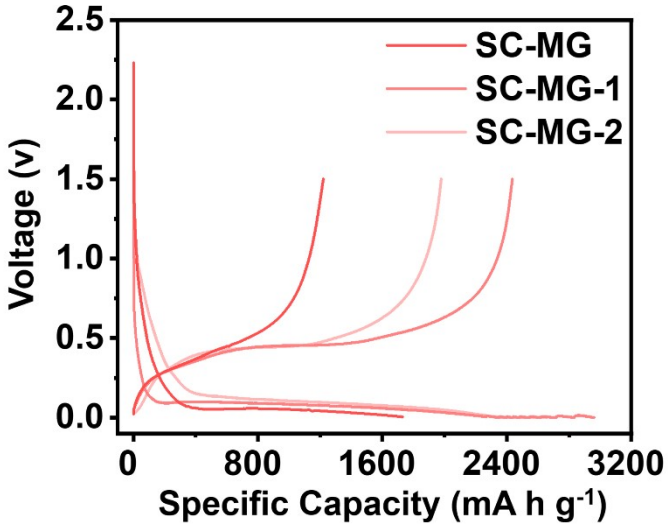

Fig. S16 Charge-discharge curves of SC-MG anodes with different proportions of SC and Mg in the first cycle.

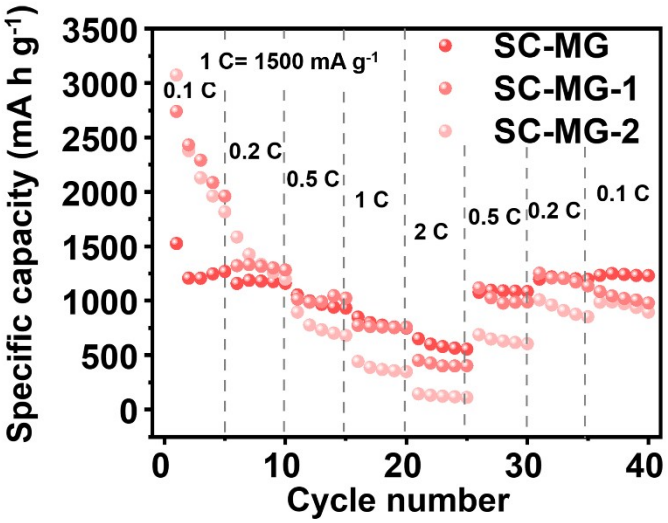

Fig. S17 Rate performance of SC-MG anodes with different proportions of SC and Mg.

Table S1 Comparison of specific surface area and total pore volume data of SC, SC-MP and SC-MG.

Sample	S_{BET} (m^2 g^{-1})	V_G (cm^3 g^{-1})
SC	1.924	0.007
SC-MP	18.733	0.067
SC-MG	29.285	0.202

Table S2 Comparison of specific surface area and total pore volume data of SC-MG with different proportions of SC and Mg.

Sample	S_{BET} (m^2 g^{-1})	V_G (cm^3 g^{-1})
SC-MG	29.285	0.202
SC-MG-1	18.394	0.111
SC-MG-2	10.188	0.042

Table S3 Comparison of EIS fitting data with different cycles of SC-MG and SC-MP anodes.

Sample	Impedance/Ω	0th	2nd	10th	50th	100th	200th	500th
	R_s	2.76	4.389	6.262	8.51	8.132	14.62	16.78
SC-MG	R_{ct}	21.38	12.68	8.185	9.692	15.86	19.78	28.63
	Z_w	20.16	11.78	23.71	20.03	31.45	157.6	240.2
	R_s	2.699	4.375	5.046	7.875	8.467	13.68	17.26
SC-MP	R_{ct}	42.46	24.56	20.42	26.73	28.48	34.64	42.08
	Z_w	25.67	14.72	27.83	45.82	70.47	250.18	960.8

Table S4. Comparison of the latest various routes of synthesizing SiO_x as anodes for LIBs.

Samples	Synthetic method	Initial Capacity/ (mA h g^{-1})	Initial CE	Cycling performance	*Ref.*
SiO_x/graphene-CMC	liquid ball milling and ultrasonic	1723.7	73.9 %	1070.2 mA h g^{-1} after 100 cycles at 200 mA g^{-1}	S1
SiO_x/SNWs@C	in-situ grown and chemical vapor deposition (CVD)	1280	~ 74.5 %	950 mA h g^{-1} for the following 300 mA g^{-1} with capacity retention >80 % over 200 cycles	S2
SiO_x/C	disproportion and high-energy ball milling	1213.9	65.7 %	1292.4 mA h g^{-1} after 100 cycles at 100 mA g^{-1}	S3
SiO_x	disproportionation and ball milling	2264.3	67.7 %	~1250 mA h g^{-1} after 50 cycles at 300 mA g^{-1}	S4
Si/SiO_x@NC	magnesiothermic reduction	1501	49 %	705 mA h g^{-1} after 100 cycles at 500 mA g^{-1}	S5
Si@SiO_x/C	magnesiothermic reduction with carbonization	2034	80.7 %	1125 mA h g^{-1} after 100 cycles at 1 A g^{-1}	S6
SiO_x	magnesiothermic reduction	1862	83 %	89.1 cycling retention after 200 cycles at 750 mA g^{-1}	S7
Si/SiO_x	magnesiothermic reduction	2224	89 %	980 mA h g^{-1} after 100 cycles at 100 mA g^{-1}	S8
SiO@C	milled and calcined	1100	51.8 %	699 mA h g^{-1} after 700 cycles at 1 A g^{-1}	S9
D-SiO@G	in situ graphene-coated by heat treatment	1937.6	78.2 %	72.4 % capacity retention after 500 cycles at 2.0 A g^{-1}	S10
TC-SiO	carbon coating with 3 wt% TiO_2	1251	71.9 %	674.5 mA h g^{-1} after 100 cycles at 0.14 A g^{-1}	S11
Porous SiO	metal-assisted chemical etching	2250	60 %	54.3 % capacity retention after 50 cycles at 0.1 C (0.15 A g^{-1})	S12

P-SiO@gl-C@F-doped C	milled and calcined	1124	60 %	772 mA h g^{-1} after 200 cycles at 0.4 A g^{-1}	S13
$Si/SiO_x/C$	restricted magnesium-vapor-reduction with and CVD	1729.6	70.6 %	943 mA h g^{-1} after 200 cycles at 750 mA g^{-1}	this work

Reference

S1. W. YongJian, T. RenHeng, L. WenChao, W. Ying, H. Ling and Liu. Ouyang, *J. Alloy. Compd.*, 2020, **830**, 154575.

S2. C. X. Shen, R. S. Fu, H. C. Guo, Y. K. Wu, C. Z. Fan, Y. G. Xia and Z. P. Liu, *J. Alloy. Compd.*, 2019, **783**, 128-135.

S3. H. Zhou, J. Z. Liu, L. S. Guo, J. Y. Zhang, S. Feng and X. M. Zhang, *Colloid. Surface A.*, 2022, **648**, 129386.

S4. Z. X. Long, R. S. Fu, J. J. Ji, Z. Y. Feng and Z. P. Liu, *Chemnanomat.*, 2020, **6**, 1127-1135.

S5. M. K. Majeed, G. Ma, Y. Cao, H. Mao, X. Ma and W. J. C. A. E. J. Ma, *Chem. Eur. J.*, 2019, **25**, 11991-11997.

S6. S. F. Liu, C. H. Kuo, C. C. Lin, H. Y. Lin, C. Z. Lu, J. W. Kang, G. T. K. Fey and H. Y. Chen, *Electrochim. Acta*, 2022, **403**, 139580.

S7. A. Raza, S. Y. Kim, J. H. Choi, J. S. Kim, M. S. Park and S. M. J. I. J. o. E. R. Lee, *Int. J. Energ. Res.*, 2022.

S8. H. Ruan, S. W. Guo, L. F. Zhang, Y. Liu, L. Li, Y. Huang, S. H. Gao and Y. F. Tian, *Ceram. Int.*, 2022, **48**, 17510-17517.

S9. J. Han, G. Chen, T. Yan, H. Liu, L. Shi, Z. An, J. Zhang and D. J. C. E. J. Zhang, *Chem. Eng. J.,* 2018, **347**, 273-279.

S10. S. Xu, J. Zhou, J. Wang, S. Pathiranage, N. Oncel, P. Robert Ilango, X. Zhang, M. Mann and X. J. A. F. M. Hou, *Adv. Funct. Mater.,* 2021, **31**, 2101645.

S11. F. Dou, L. Shi, P. Song, G. Chen, J. An, H. Liu and D. J. C. E. J. Zhang, *Chem. Eng. J.,* 2018, **338,** 488-495.

S12. J.-I. Lee and S. J. N. E. Park, *Nano Energy,* 2013, **2,** 146-152.

S13. M. Wang, L. Yin, M. Li, S. Luo, C. J. J. o. c. Wang and i. science, *J. Colloid Interf. Sci.,* 2019, **549,** 225-235.